

Seasonality in SST-Forced Atmospheric Short-Term Climate Predictability

X. W. QUAN, P. J. WEBSTER, A. M. MOORE, AND H. R. CHANG

Program in Atmospheric and Oceanic Sciences, University of Colorado, Boulder, Colorado

(Manuscript received 29 May 2003, in final form 28 February 2004)

ABSTRACT

The seasonal dependence of atmospheric short-term climate (i.e., seasonal to interannual) predictability is studied. This is accomplished by analyzing the output from ensemble integrations of the European Centre for Medium-Range Weather Forecasts model. The integrations use the observed evolution of sea surface temperature (SST) as prescribed boundary forcing. Forced by the interannual variation of SST, the short-term climate predictability of the atmospheric circulation is geographically and seasonally dependent. In general, the predictability is larger in the Tropics than the extratropics and is greater in the Pacific–Atlantic Ocean sector compared to the Indian Ocean–Asian monsoon region. Predictability is also higher in the winter hemisphere than in the summer hemisphere. On average, the weakest predictability in the Northern Hemisphere occurs during the northern autumn. However, it is noted that the 1982/83 strong El Niño event produced stronger atmospheric predictability than the 1988/89 strong La Niña event during the northern spring, and the predictability pattern is reversed during the northern autumn.

Predictability is further partitioned into its internal and external components. The external component is defined as the interannual variation of ensemble average, and the internal component is the sample-to-sample variance. The temporal and spatial structure in the external variability accounts for most of the structure in the SST-forced atmospheric predictability. However, there are regions in the Tropics, such as over the monsoon region, where the external and internal variabilities show roughly the same magnitude. Overall, internal variability is largest in the extratropics. Specifically, the internal variability is larger in the northern extratropics during the northern autumn and larger in the southern extratropics during the northern spring. In contrast, the external variability is smaller (larger) in the northern extratropics during the northern autumn (spring).

It is concluded that major features of the SST-forced atmospheric predictability are determined by the external variability in the Tropics. In the extratropics, the predictability is determined by seasonal variations in both internal and external variabilities. The weakest predictability that occurs in the northern extratropics during the northern autumn is the result of a conjunction of a local increase in internal variability and a decrease in external variability at the same time.

Furthermore, the external variability is controlled by seasonality in the forcing over the tropical Pacific Ocean, which is largely determined by the following two mechanisms: 1) the annual cycle–ENSO interaction over the tropical Pacific Ocean and 2) nonlinear effects of hydrological processes associated with the annual cycle–ENSO interaction. Also, it is interesting that the annual cycle–ENSO interaction can be summarized into a conceptual model that shows some analogy to the quark model in nuclear physics.

1. Introduction

Starting with the pioneering work by Richardson (1922), numerical models have quickly become powerful tools to simulate and predict the evolution of the atmosphere (e.g., Charney 1949; Charney et al. 1950; von Neumann and Ritchmyer 1950; Charney and Philips 1953; Philips 1959; Lorenz 1960; Kurihara 1965; Smagorinsky et al. 1965; Kasahara and Washington 1967; Shuman and Hovermale 1968; Arakawa 1972; among others). With these tools, skillful predictions of weather variations up to 6 days in advance were demonstrated during the 1960s (e.g., Miyakoda et al. 1972), and skill-

ful predictions up to 10 days in advance are now possible (e.g., Lorenz 1982; Dalcher and Kalnay 1987; Palmer and Tibaldi 1988; Chen 1989; Schubert and Suarez 1989; Tracton et al. 1989; Van den Dool 1994; among others). The upper limit of the numerical weather prediction is determined by the sensitivity of model predictions to initial conditions. The sensitivity exists inevitably because of the chaotic nature of the atmosphere (e.g., Lorenz 1963), which leads to the rapid growth of small errors in the initial conditions (e.g., Reynolds et al. 1994).

To assess the predictability of atmospheric variations for longer than 10 days, one needs to include an appropriate estimation of the predictability of boundary conditions (e.g., Shukla 1981). In the remainder of this paper, we will evaluate the “potential” atmospheric seasonal predictability assuming “perfect” SST prediction.

Corresponding author address: Dr. Xiao-Wei Quan, NOAA–CIRES CDC, R/E/CD1, 325 Broadway, Boulder, CO 80305.
E-mail: quan.xiaowei@noaa.gov

The atmospheric short-term climate (i.e., seasonal to interannual) predictability that will be subsequently discussed is evaluated from ensemble climate simulations with an atmospheric general circulation model (AGCM) using prescribed variations of global SST for the 14-yr period from 1979 to 1992.

The sensitivity to initial conditions in such climate simulations is different from that in weather forecasts. This is because the growth of initial error is not crucial in short-term climate prediction, as it is in weather forecasting. The study by Borges and Sardeshmukh (1995) suggested that in a free atmosphere without external (boundary) forcing, a small perturbation can maintain its growth for less than 12 days. This seems to be the upper limit for error growth in a free atmosphere. Therefore, reliability of a seasonal prediction depends on whether the atmospheric response to boundary forcing is large enough to overcome the maximum uncertainty arising from initial errors.

As a boundary forcing, SST variation in the tropical Pacific Ocean is a source of atmospheric short-term predictability because of the existence of the El Niño–Southern Oscillation (ENSO), a robust climate phenomenon over the tropical Pacific Ocean that generates global-scale atmospheric impacts (e.g., Philander 1990; Diaz and Markgraf 2000). Figure 1 shows the standard deviation of the interannual variations of SST for four seasons. The most remarkable feature in Fig. 1 is the large interannual SST variability in the eastern tropical Pacific Ocean, which acts as a strong boundary forcing for atmospheric circulation. During the last few decades, there have been significant advances in understanding ENSO. The development of a comprehensive observation system and better statistical and numerical models have made the prediction of ENSO more reliable (e.g., Webster and Palmer 1997; Wallace et al. 1998). Based on the success of the prediction of ENSO, researchers have started to make experimental seasonal-to-interannual predictions for regions outside the tropical Pacific region. In practice, seasonal-to-interannual predictions are often made as two-tiered processes: a prediction of SST anomalies followed by a prediction of atmospheric response to those SST anomalies (e.g., Anderson et al. 1999). As such, the issue of predictability of short-term climate variation can be considered as two related subissues: the predictability of the seasonal-to-interannual variations in SST and the predictability of atmospheric circulation in the presence of SST forcing. The atmospheric predictability we examine in this paper is based on the boundary forcing of observed SST variations and therefore represents only the potential atmospheric predictability for the scenario of perfect SST prediction.

It is well known that atmospheric predictability is generally larger in the Tropics than in the extratropics (Charney and Shukla 1981; Palmer and Anderson 1994). This difference arises from the greater dependence on the lower boundary forcing in the Tropics compared to

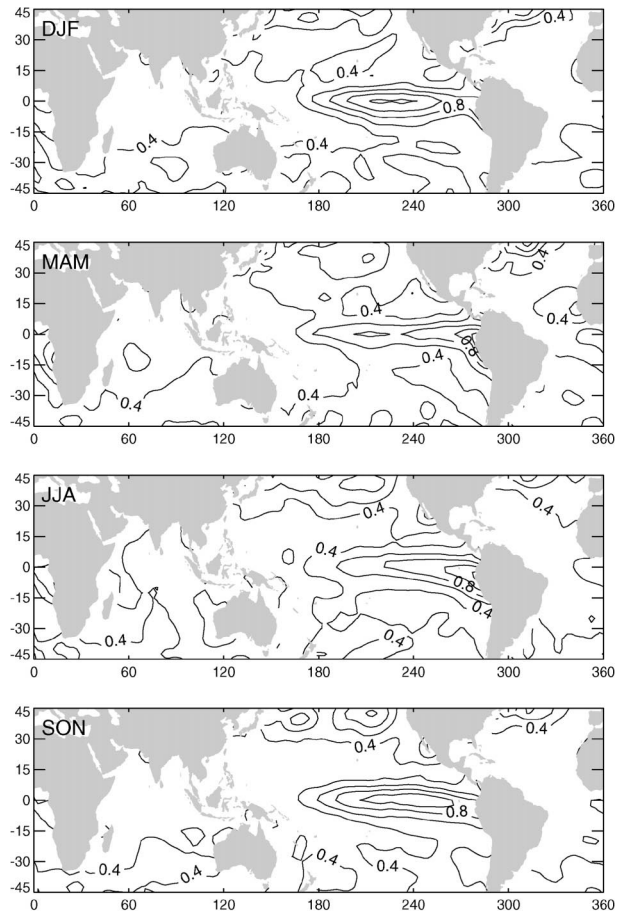


FIG. 1. Std dev of the interannual variations in SST. Contours start from 0.2°C with a contour interval of 0.2°C.

the extratropics. Charney and Shukla (1981) hypothesized that this difference occurs because of the general lack of hydrodynamical instability in the Tropics compared to the extratropics. The growth of instabilities is so vigorous at higher latitudes that the flow is essentially chaotic. However, there are regions in the Tropics that appear less predictable than others. To account for this, it has been hypothesized (e.g., Palmer 1994; Webster et al. 1998) that the monsoon region, for example, possesses instability modes that render the monsoon circulation more chaotic than other regions of the Tropics. The chaotic nature of some regions of the globe means that the system is locally sensitive to initial conditions, even in the Tropics. Nonetheless, ENSO-forced atmospheric predictability at seasonal-to-interannual time scales is affected by both initial and boundary conditions. By changing the statistics of the Pacific–North American (PNA) atmospheric circulation pattern (e.g., Horel and Wallace 1981; Hoskins and Karoly 1981), SST variations in the tropical Pacific Ocean may increase the short-term climate predictability of atmospheric variations outside the Tropics. Being sensitive

to both initial and boundary conditions is a unique property of the SST-forced atmospheric prediction at seasonal-to-interannual time scales.

The extratropical response to tropical forcing varies significantly from one season to another. Many previous studies addressing the mechanism of tropical–extratropical interactions have considered the Northern Hemisphere winter period because tropical influences are much more significant at this time of year (e.g., Webster 1982; Blackmon et al. 1983; Shukla and Wallace 1983; Lau 1985; among others). Recent studies indicate a further stratification in atmospheric predictability: in the Northern Hemisphere, seasonal atmospheric predictability is generally larger during the spring than the autumn (e.g., Brankovic et al. 1994; Brankovic and Palmer 1997; Livezey et al. 1997; Rowell 1998; Kumar and Hoerling 1998).

It has also been noticed that season-to-season variations in atmospheric predictability during El Niño years are, in general, different from those found during La Niña years. Chen and Van den Dool (1997) concluded that in the region covered by the PNA pattern, a high level of predictability is seen from December to April during El Niño years. During La Niña years the predictability drops to below normal from November to March. The spring barrier in the atmospheric predictability is a distinct phenomenon for the La Niña phase of the ENSO cycle.

This study attempts to determine the mechanisms that produce seasonality in the SST-forced atmospheric predictability. Data and methods are described in section 2. The seasonality of the SST-forced atmospheric predictability is discussed in greater detail in section 3. Mechanisms are discussed in section 4, and conclusions are given in section 5.

2. Data and methods

In this paper, we study the SST-forced atmospheric predictability by analyzing the output of AGCM ensemble seasonal forecasts and observed fields. The data used are products of a European research project on seasonal-to-interannual forecasting called the Prediction of Climate Variations on Seasonal-to-Interannual Timescales (PROVOST). The data are available on CD-ROMs prepared by the European Centre for Medium-Range Weather Forecasts (ECMWF; Becker 1997).

The ECMWF AGCM is a T63L31 version with a cycle-13r4 scheme of model physics. The model's horizontal resolution is about 1.9° latitude \times 1.9° longitude and has 31 vertical layers. The model output consists of 59 ensembles of 120-day integrations driven by the observed SST for the 59 seasons during the period from January 1979 to December 1993. Each ensemble has nine members of 120-day integrations forced by the same SST, but commenced with different atmospheric initial conditions. For example, for the 120-day ensemble of the December–March of 1992/93, individual

members are generated identically using the same evolving SST of this season, but beginning from different initial conditions starting separately at 1200 UTC 22 November, 1200 UTC 23 November . . . 1200 UTC 30 November. Ensemble simulations for each of the 59 seasons were generated in the same way.

In addition to the PROVOST project model output, ECMWF reanalysis data are also available on the same CD-ROMs. The reanalysis dataset covers the 14-yr period from January 1979 to December 1992.

The original PROVOST data are available in the form of 10-day means. However, all the analyses presented in this paper are based on seasonal means of winter [December–February (DJF)], spring [March–May (MAM)], summer [June–August (JJA)], and autumn [September–November (SON)]. Thus, a variable can be defined by $X_{s,y,n}$, in which the subscript $s = 1, 4$ represents season, $y = 1979, 1993$ represents year, and $n = 1, 9$ indicates which sample in the ensemble the variable belongs to.

When analyzing prescribed SST AGCM simulations, we consider the SST as external forcing and the AGCM as an open system that is influenced by that forcing. We also consider the sensitivity to external forcing as a measure of predictability, whereas we consider the sensitivity to atmospheric initial condition (internal dynamics) as a measure of uncertainty in predictions. We define external variability as the variability forced by external forcing and internal variability as the variability of the system due to its internal dynamics. Thus, forced predictability of the open system can be measured by how the system's external variability compares to its internal variability.

For a given season, the internal variability of an AGCM is measured by the differences among sample integrations and defined as R_I (see Table 1):

$$R_I = \frac{1}{Y} \sum_{y=1}^Y \sigma_y^2, \quad (1)$$

where $Y = 14$ is the number of years for which the model is integrated, and σ_y^2 is the internal (i.e., sample to sample) variability of X in the y th year given by

$$\sigma_y^2 = \frac{1}{N-1} \sum_{n=1}^N (X_{y,n} - [X_y])^2. \quad (2)$$

Here, $[X_y]$ is the ensemble mean of X in the y th year,

$$[X_y] = \frac{1}{N} \sum_{n=1}^N X_{y,n}, \quad (3)$$

where $N = 9$ is the total number of sample integrations in each ensemble. For a given season, the subscript s is constant, and we therefore omit it for clarity.

External variability of an AGCM is measured by the interannual variability of the ensemble mean and is defined as R_E :

$$R_E = \frac{1}{Y-1} \sum_{y=1}^Y ([X_y] - \overline{[X]})^2, \quad (4)$$

TABLE 1. Definition of R_I and R_E for a season.

	Year = 1	Year = 2	Year = 3	...	Year = y	→	Time - mean	
Sample = 1	$X_{1,1}$	$X_{2,1}$	$X_{3,1}$...	$X_{y,1}$	→	\bar{X}_1	
Sample = 2	$X_{1,2}$	$X_{2,2}$	$X_{3,2}$...	$X_{y,2}$	→	\bar{X}_2	
Sample = 3	$X_{1,3}$	$X_{2,3}$	$X_{3,3}$...	$X_{y,3}$	→	\bar{X}_3	
⋮	⋮	⋮	⋮	⋮	⋮		⋮	
⋮	⋮	⋮	⋮	⋮	⋮		⋮	
Sample = n	$X_{1,n}$	$X_{2,n}$	$X_{3,n}$...	$X_{y,n}$	→	\bar{X}_n	
↓	↓	↓	↓	...	↓		↓	
Ensemble - mean	$[X_1]$	$[X_2]$	$[X_3]$...	$[X_y]$	→	$[\bar{X}]$	→ R_E
	↓	↓	↓	...	↓			
	σ_1^2	σ_2^2	σ_3^2	...	σ_y^2	→	R_I	

where $[\bar{X}]$ is the climatological mean of the ensemble mean:

$$[\bar{X}] = \frac{1}{Y} \sum_{y=1}^Y [X_y]. \tag{5}$$

The SST-forced atmospheric predictability can be measured by the ratio of how the AGCM’s external variability compares to its internal variability:

$$r = \frac{R_E}{R_I}. \tag{6}$$

Since R_I can be very small, while R_E is large over a region of strong SST forcing (e.g., over the tropical Pacific Ocean), which may cause the ratio r to vary in a range as wide as from 0 to ∞ , it is convenient to introduce a normalized measure—the ratio of external variability to the sum of external and internal variabilities:

$$R = \frac{R_E}{R_I + R_E} = \frac{r}{1 + r}. \tag{7}$$

Here, R varies within the range from 0 to 1 and therefore provides a uniform measure of predictability, and $R = 0$ indicates no external variability ($R_E = 0$); the system has no predictability. When $0 < R < 0.5$ (i.e., $0 < R_E < R_I$), the system has, in general, low potential predictability but may exhibit high potential predictability for individual cases of extreme external forcing. When $R > 0.5$ (i.e. $R_E > R_I$), the influence from external forcing is usually larger than internal variability, and the system is judged to have high potential predictability. Also, $R = 1$ indicates no internal variability ($R_I = 0$), meaning that the system is perfectly predictable—it responds deterministically to any changes in external forcing. Note that the conversion between r and R is nonlinear; when $R > 0.5$ a small increase in R means a much larger increase in the ratio r (Table 2).

TABLE 2. The predictability factors R and r .

R	0.1	0.2	0.3	0.4	0.5	0.6	0.7	0.8	0.9
r	0.1	0.2	0.4	0.7	1.0	1.5	2.3	4.0	9.0

However, R is only a measure of the potential predictability of an AGCM. A large value of R only means a small difference among each sample of ensemble forecasts subjected to identical SST forcing. There is no assurance of simulated behavior in nature since limited sampling does not permit construction of perfect analysis. Also, it is necessary to note that $R = 1$ only means that an open system is as predictable as its external forcing. One may further divide the interannual variability of external forcing (SST) as $V_{SST} = V_{ENSO} + V_{noise}$ where V_{ENSO} represents the magnitude of ENSO, and V_{noise} represents the magnitude of non-ENSO SST variabilities. The predictability of the variation in SST due to ENSO may be measured by another signal-to-noise ratio, $r_{SST} = V_{ENSO}/V_{noise}$ (Trenberth 1984). In the rest of this paper, we assume that the time variation of SST is known (perfect prediction), and we focus on the SST-forced atmospheric predictability (R).

For any season, the year-to-year variation in the SST-forced atmospheric predictability can be seen by estimating the signal-to-noise ratio for each year (y):

$$r_y = \frac{([X_y] - [\bar{X}])^2}{\sigma_y^2} \quad \text{and} \tag{8}$$

$$R_y = \frac{r_y}{1 + r_y}. \tag{9}$$

3. Seasonality in the SST-forced atmospheric predictability

a. Predictability (R)

The values of R for 850- and 200-mb zonal wind fields of the ECMWF AGCM are shown in Fig. 2. Comparing with Fig. 1, one may easily see that in the Tropics the large values of R are centered around the regions of large SST variations. The predictability is greater over the tropical Pacific and Atlantic Oceans than over the tropical Indian Ocean. In the extratropics, the spatial distribution of large values of R has strong seasonal dependence. The predictability is larger in the winter hemisphere (i.e., the Northern Hemisphere during DJF

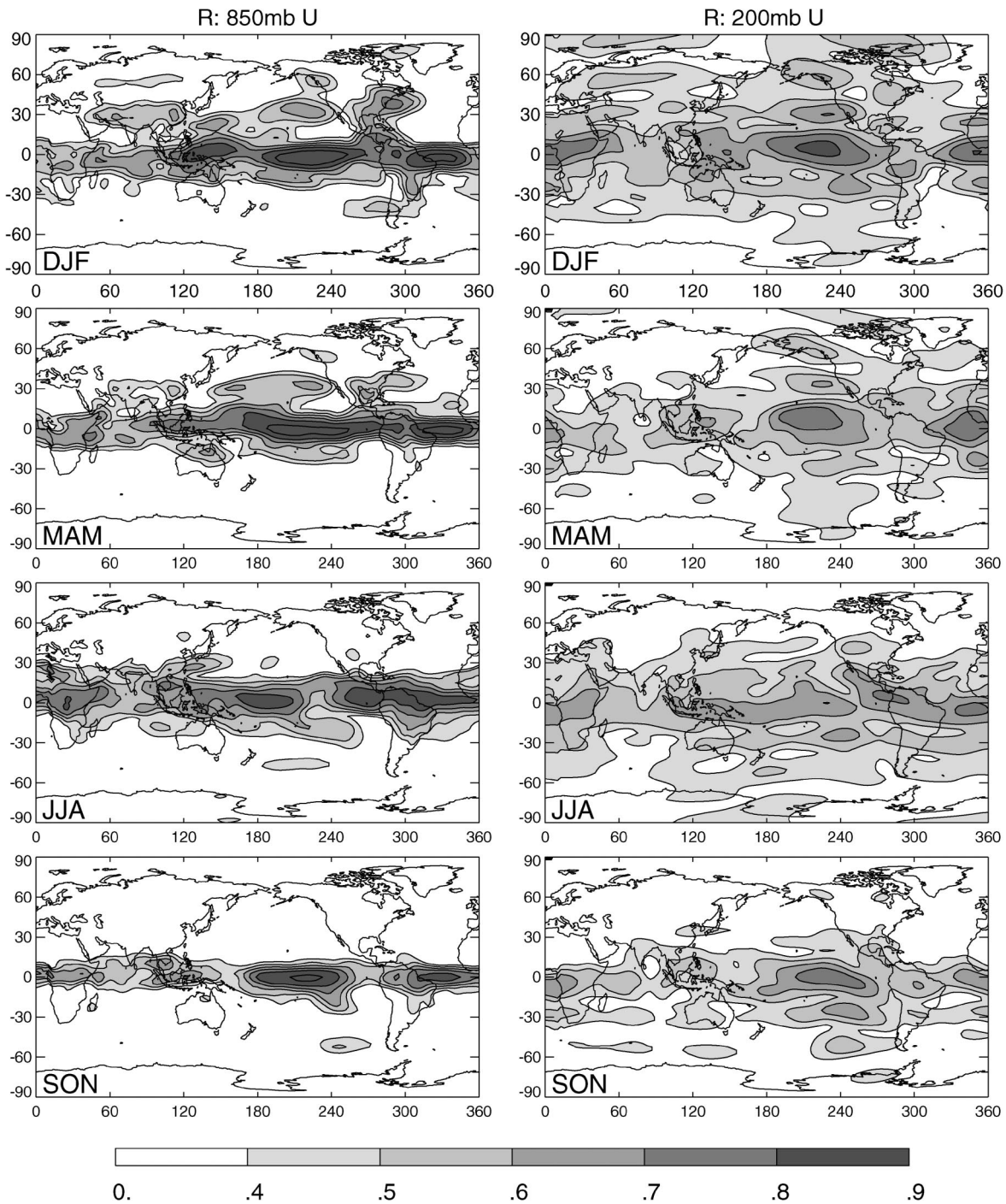


FIG. 2. Potential predictability (R) of the 850- and 200-mb zonal wind defined using the ECMWF AGCM model result. Contours start from 0.4°C with a contour interval of 0.1°C.

and the Southern Hemisphere during JJA) than in the summer hemisphere. Also, during the northern fall (SON), the predictability is smallest in the northern extratropics.

Moreover, one may examine the temporal variation in the SST-forced atmospheric predictability using Eq.

(9). Figure 3 shows the interannual variation in the predictability factor (R) of the 200-mb zonal wind over the Pacific–American sector (120°E – 60°W). In the northern extratropics (30° – 90°N), the predictability for the northern fall is weak and has little interannual variation throughout the 14-yr period from 1979 to 1992. The

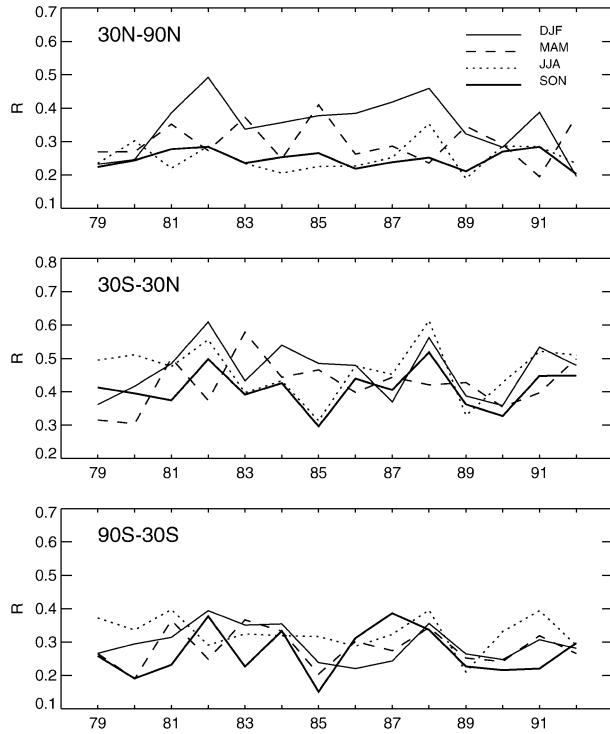


FIG. 3. Potential predictability (R) of the 200-mb zonal wind defined using the ECMWF AGCM model result: interannual variation of spatial mean over the Pacific–American sector ($120^{\circ}\text{E}–60^{\circ}\text{W}$).

TABLE 3. Predictability factors R , R_f , and R_E for the 200-mb zonal wind over the Pacific–American region ($120^{\circ}\text{E}–60^{\circ}\text{W}$).

	DJF	MAM	JJA	SON
30°–90°N				
R	0.31	0.28	0.26	0.23
R_f	0.96	0.85	0.81	0.95
R_E	0.53	0.40	0.31	0.31
30°S–30°N				
R	0.44	0.44	0.45	0.38
R_f	0.73	0.68	0.74	0.72
R_E	0.73	0.64	0.74	0.50
90°–30°S				
R	0.29	0.27	0.29	0.25
R_f	0.77	0.95	1.07	0.91
R_E	0.37	0.41	0.57	0.37

predictability has larger interannual variation in the Tropics ($30^{\circ}\text{S}–30^{\circ}\text{N}$) and southern extratropics ($90^{\circ}–30^{\circ}\text{S}$). However, on average over the 14-yr period, relative minimum predictabilities also occur during the northern fall compared locally to other seasons in the Tropics and southern extratropics of the Pacific–American sector, although the predictabilities in the tropical and southern extratropical regions are still higher than their counterparts in the northern PNA sector in this season (cf. Table 3).

Chen and Van den Dool (1997) noticed that in the region covered by the PNA pattern ($20^{\circ}–70^{\circ}\text{N}$, $120^{\circ}–60^{\circ}\text{W}$), the annual cycle of atmospheric predictability during El Niño years is generally different from its counterpart during La Niña years. The asymmetry between the annual cycle in the SST-forced atmospheric predictability during El Niño and that during La Niña years may also be seen in Fig. 4, which shows the season-to-season variation in the predictability factor (R) of the 200-mb zonal wind over the Pacific–American sector for the five seasons of a strong El Niño event (from JJA 1982 to JJA 1983) and five seasons of a strong La Niña event (from JJA 1988 to JJA 1989). A difference between the El Niño and La Niña regarding the annual cycle in predictability appears in the Tropics ($30^{\circ}\text{S}–30^{\circ}\text{N}$) and southern extratropics ($90^{\circ}–30^{\circ}\text{S}$). In these two regions, the predictability factor R during the JJA and/or SON of the first year of the El Niño event is

lower than the R during the following DJF and MAM, and the pattern is somewhat reversed for the La Niña event. The differences between the predictability factors for MAM in the El Niño and La Niña are larger than 2.3 standard deviations and statistically significant at 95% confidence level in both the Tropics and southern extratropics. We also notice that the predictability is higher in DJF and MAM than in JJA and SON in the northern extratropics during both the warm and cold events, which is an exception to the opposite trends in

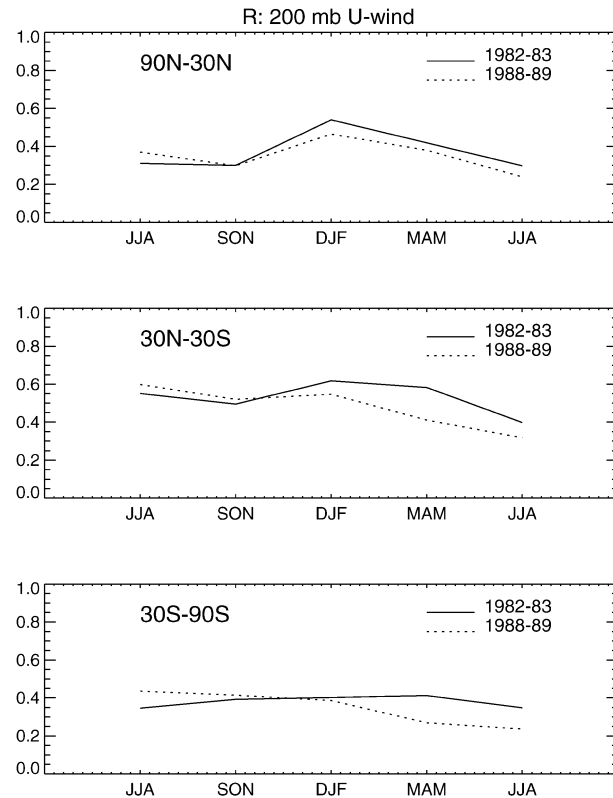


FIG. 4. Same as in Fig. 3 but for season-to-season variation.

the predictability in the warm and cold events, as those appear in the Tropics and southern extratropics.

To understand the mechanisms that determine the SST-forced atmospheric predictability, it is helpful to partition the predictability into its internal and external components and examine each of them separately.

b. Internal variability (R_I) and external variability (R_E)

The role of the internal and external variabilities [Eqs. (1) and (2)] in the determination of the SST-forced atmospheric predictability may be seen by comparing their spatial distribution with the pattern of the predictability. The spatial patterns of the internal and external variabilities in the 200-mb zonal wind field are shown in Fig. 5. It is seen that the magnitude of the internal variability in the 200-mb zonal wind field is nonzero (larger than 1 m s^{-1}) almost everywhere in the entire globe (Fig. 5, left). Centers of maximum internal variability appear in the midlatitudes of both hemispheres. The spatial pattern of the internal variability shows little season-to-season change, but the magnitude is slightly larger in the northern midlatitudes during SON and DJF and in the Southern Hemisphere during MAM and JJA. The spatial pattern of the internal variability is quite different from the pattern of the predictability factor R .

On the other hand, the spatial pattern of the external variability (Fig. 5, right) is similar to the pattern of R (Fig. 2, right). All of the major features in the predictability pattern may find corresponding parts in the spatial pattern of the external variability. For example, the seasonality in the SST-forced atmospheric planetary wave (e.g., Webster 1982) is apparently responsible for the similar pattern in the spatial distribution of the predictability factor R . Recall from Fig. 4 that the El Niño (La Niña) signal had strong seasonal variation with the potential predictability weaker in JJA and SON than in DJF and MAM in the northern extratropics, but the potential predictability is higher in JJA (SON) than DJF (SON) in the Tropics and the southern extratropics during the cold event. Figure 5 explicitly shows that the northern extratropical exception is attributed to the seasonality in the SST-forced planetary waves (Webster 1982). Therefore, the external variability (i.e., atmospheric response to the variation in SST) is the major factor that contributes to the atmospheric predictability in the seasonal-to-interannual time scale.

The contributions of the external and internal variabilities to the SST-forced atmospheric seasonal predictability are further illustrated in Fig. 6, which shows the zonal average of R , R_E , and R_I for the 850- and 200-mb zonal wind fields. Again, the maxima in the Tropics and the minima in the northern extratropics during the northern fall are two remarkable features in the zonal average of R in both the lower and upper troposphere (Fig. 6, top). The tropical maxima in the predictability

factor R may be attributed to the contributions from both the high external and low internal variabilities. The annual migration of the maximum in R_E in the lower troposphere shows that the largest external variability occurs in the intertropical convection zone (ITCZ), and the seasonal predictability is linked to SST forcing via the interannual variation of precipitation inside ITCZ. The maxima of the internal variability R_I (Fig. 6, bottom) in the midlatitudes contribute to a decrease in the predictability in the extratropical zone. The fall (SON) minima of the predictability in the northern extratropics may also be attributed to the weakening of external variability because the season-to-season variation in the predictability factor R follows the pattern of variation in the external variability R_E .

A quantitative comparison among the seasonal variations in R_I , R_E , and R of the 200-mb zonal wind over the Pacific–American sector (120°E – 60°W) is given in Table 3. In the Tropics (30°S – 30°N), a minimum R of 0.38 occurs during SON due to the fact that R_E is a minimum then. In the Tropics, the season-to-season variation in the internal variability R_I is much smaller compared to its counterpart in the external variability R_E . In the northern extratropics (30° – 90°N), R_E has the same value of 0.31 during both JJA and SON, which is lower than the 0.53 value found during DJF and the 0.40 value found during MAM. In the northern extratropics, R reaches a minimum during autumn because the value of R_I during SON, 0.95, is much higher than the R_I during JJA, 0.81. Similarly, in the southern extratropics (30° – 90°S), the R_E has the lowest value, 0.37, during both SON and DJF, and the SON minimum R is the result of a larger R_I , 0.91, during SON than the R_I of 0.77 during DJF. Therefore, the SON weakening in R is mainly caused by the weakening in external variability in the Tropics. And, in the extratropics, the SON weakening in R is due to both the decrease in external variability and the increase in internal variability during this season.

4. Why does the predictability differ between El Niño and La Niña?

As shown in the above section (Fig. 4), it appears that the SST-forced atmospheric predictabilities are larger for the northern spring (MAM) than fall (SON) during an El Niño year, and the pattern is reversed in the Tropics and southern extratropics during a year of La Niña. Such asymmetry between the seasonalities of the SST-forced atmospheric predictability during El Niño and La Niña years may be a manifestation of the seasonality in the external forcing of the tropical Pacific SST because it can be mostly explained by the mechanisms that determine the strength of SST forcing in the tropical Pacific Ocean and its atmospheric response.

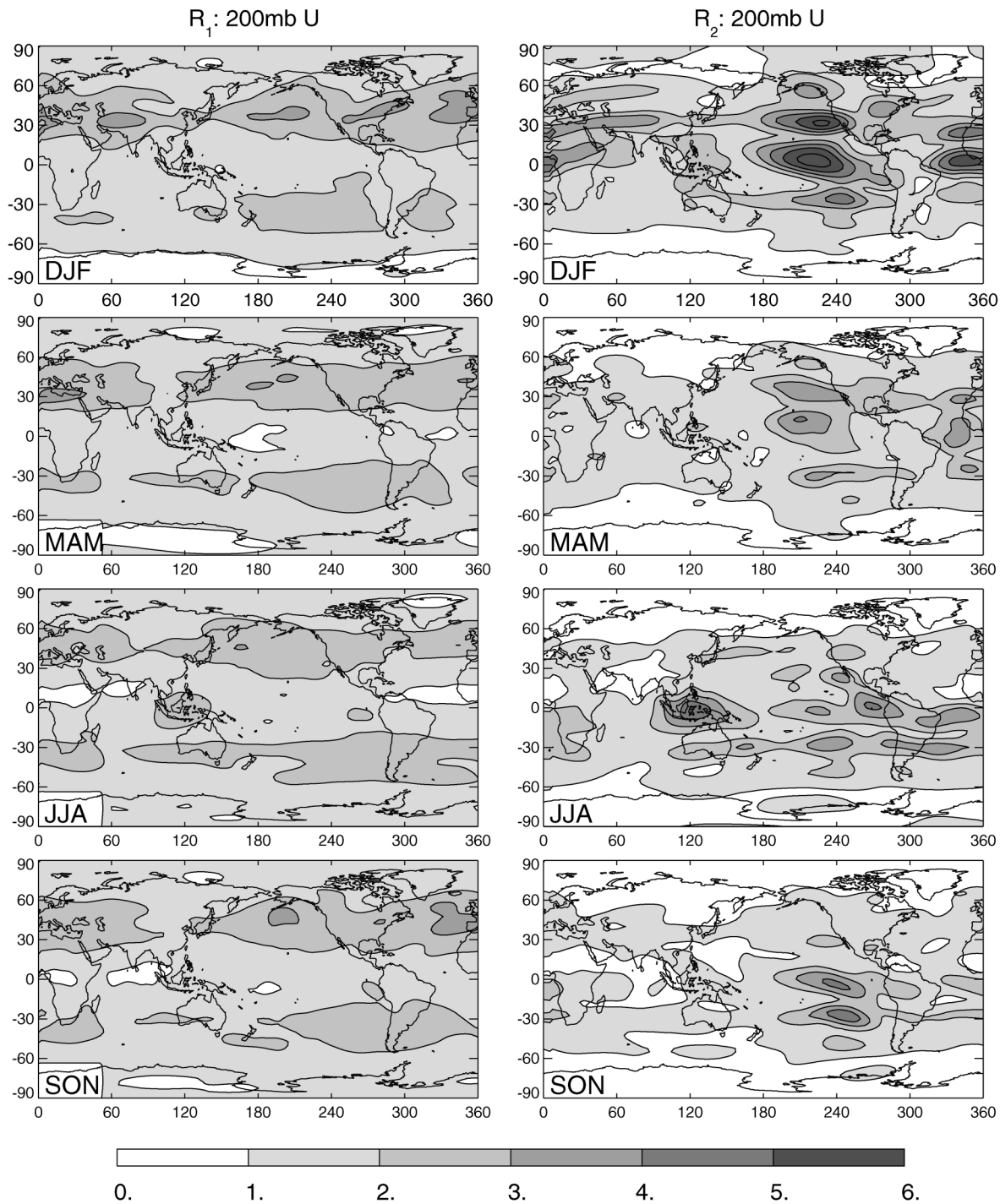


FIG. 5. Internal (R_1) and external variability (R_2) of the 200-mb zonal wind defined using the ECMWF AGCM model result. Contours start from 1 m s^{-1} with a contour interval of 1 m s^{-1} .

a. The annual cycle and ENSO anomalies

It is helpful to introduce the definition of the annual cycle anomaly and ENSO anomaly. For some variable X , the seasonal mean value for the season s of year y can be written as:

$$X_{s,y} = \bar{X}_s + X'_{s,y} + \text{noise},$$

where $X'_{s,y}$ is the anomaly of interannual variation due to ENSO and is abbreviated as “ENSO anomaly.” Variations due to other causes, such as the variabilities of intraseasonal and/or other time scales, the model’s sen-

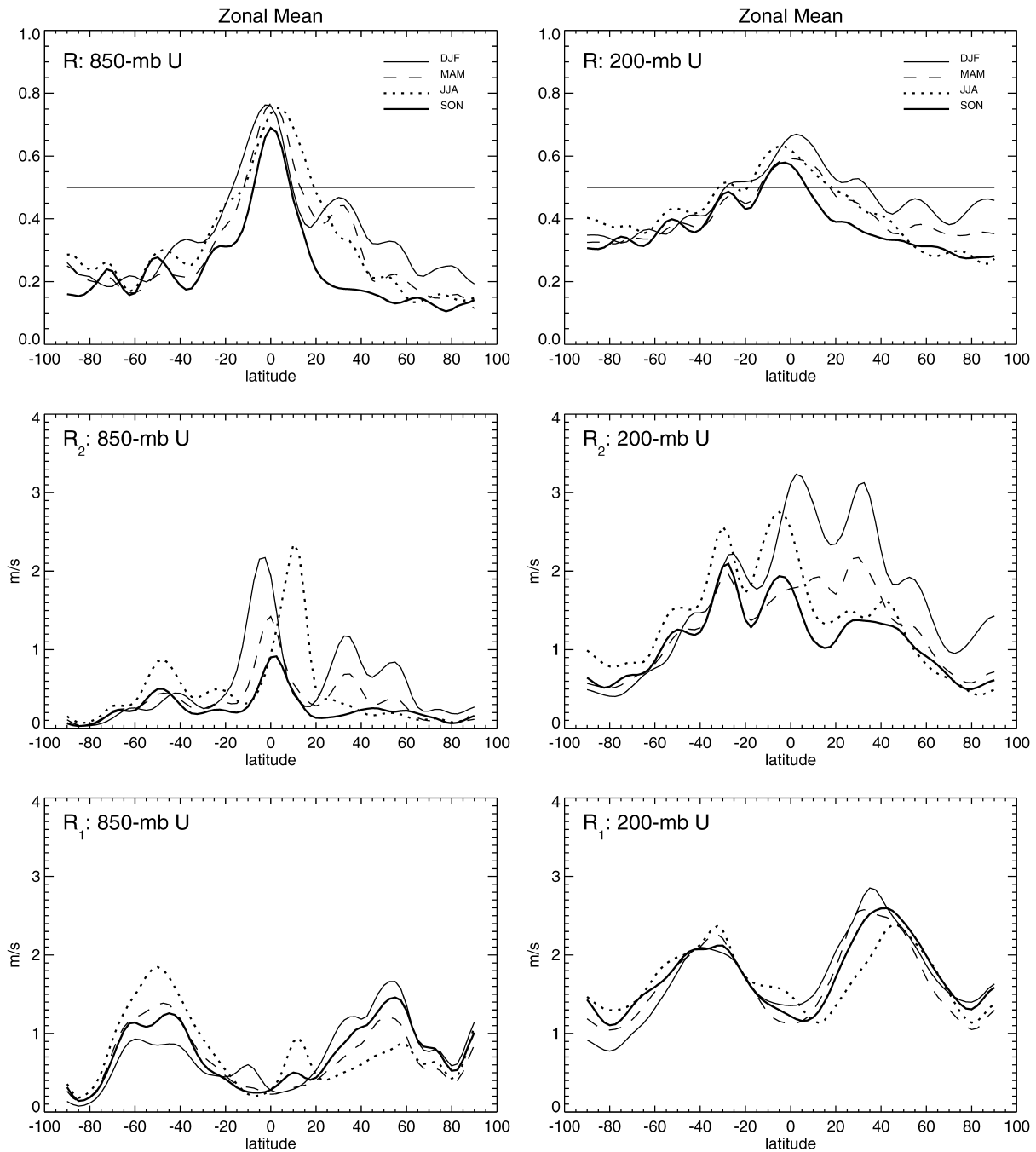


FIG. 6. Zonal mean of the predictability factors R , R_1 , and R_2 of the 850- and 200-mb zonal wind defined using the ECMWF AGCM model result.

sitivity to initial condition, and model errors, are considered as noise. Here, \bar{X}_s represents the climatological mean for season s written as

$$\bar{X}_s = \frac{1}{14} \left(\sum_{y=1}^{14} X_{s,y} \right)$$

and can be further written as

$$\bar{X}_s = \bar{\bar{X}} + \bar{X}'_s,$$

where

$$\bar{\bar{X}} = \frac{1}{4} \left(\sum_{s=1}^4 \bar{X}_s \right) = \frac{1}{56} \left(\sum_{y=1}^{14} \sum_{s=1}^4 X_{s,y} \right)$$

is a constant representing the annual average of the cli-

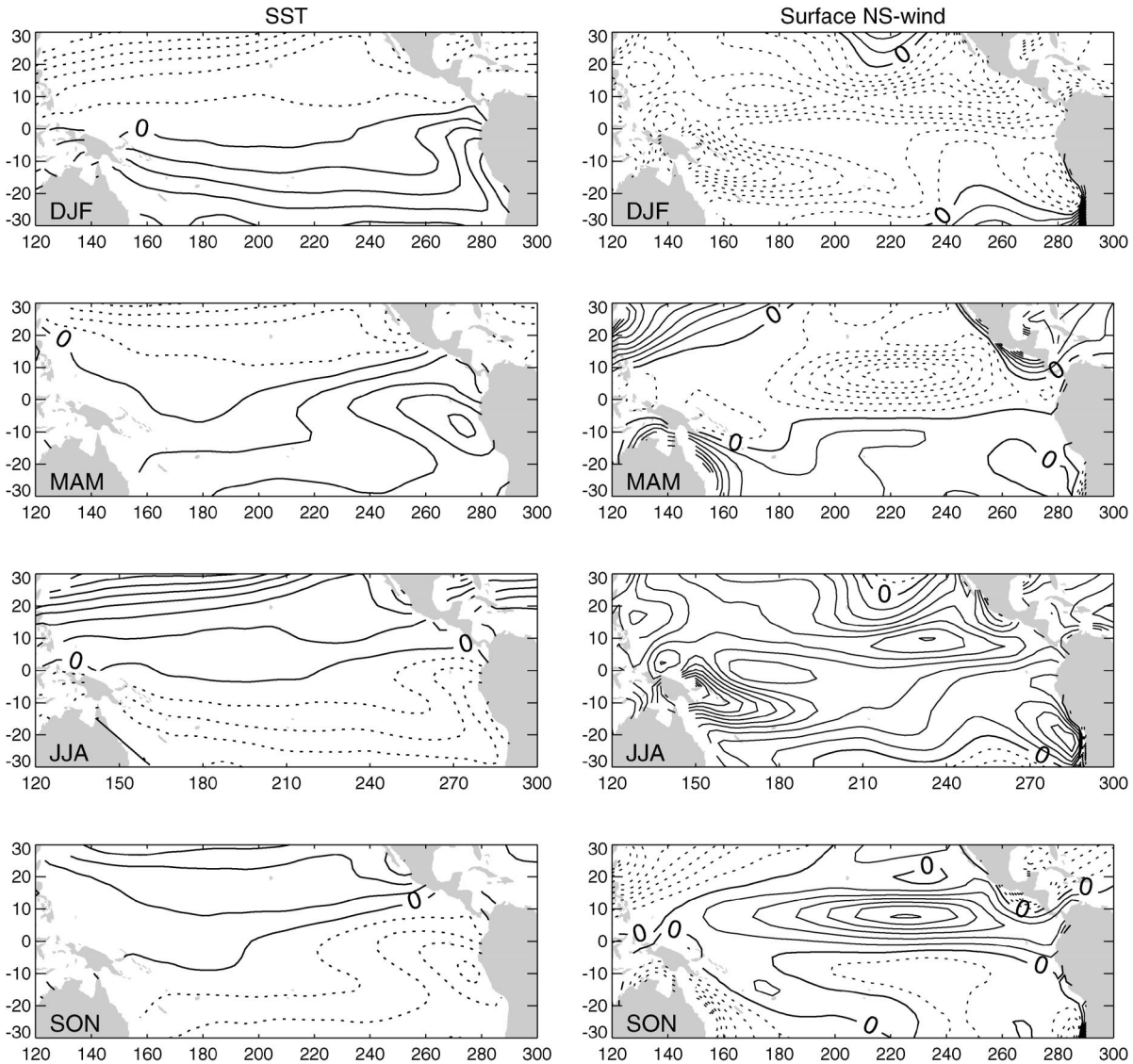


FIG. 7. The annual cycle anomalies of (left) SST and (right) the meridional component of surface wind. Contours start from 0°C with a contour interval of $\pm 0.5^{\circ}\text{C}$ for SST and $\pm 0.5\text{ m s}^{-1}$ for surface wind.

matological means of each season (\bar{X}_s), and $\bar{X}'_s = \bar{X}_s - \bar{X}$ is the anomaly due to the climatological mean annual cycle and abbreviated as “annual cycle anomaly.” Thus, the seasonal mean of a variable, $X_{s,y}$, can be expressed as the sum of the long-term climatological mean (\bar{X}) and the annual cycle anomaly (\bar{X}'_s) plus the ENSO anomaly ($X'_{s,y}$) plus noise:

$$X_{s,y} = \bar{X} + \bar{X}'_s + X'_{s,y} + \text{noise}. \quad (10)$$

We choose to use SST, the meridional component of surface wind, and precipitation for the analysis in this section because the three variables represent three key aspects of the air–sea interaction over the tropical Pacific Ocean: boundary forcing, local dynamic response (convergence/divergence), and local thermodynamic response (diabatic heating) in the atmosphere. The spatial

pattern of the annual cycle anomalies (\bar{X}'_s) of the SST and the meridional component of surface wind are shown in Fig. 7. In the tropical Pacific, the SST has a strong annual cycle (Fig. 7, left). Regulated by the annual cycle in solar radiation, the SST is warmer in the Niño-1 ($10^{\circ}\text{--}5^{\circ}\text{S}$, $90^{\circ}\text{--}80^{\circ}\text{W}$) and Niño-2 ($5^{\circ}\text{S}\text{--}0^{\circ}$, $90^{\circ}\text{--}80^{\circ}\text{W}$) region during DJF. A warm SST extends westward further into the region of Niño-3 ($5^{\circ}\text{S}\text{--}5^{\circ}\text{N}$, $150^{\circ}\text{--}90^{\circ}\text{W}$) during MAM, which makes the east–west gradient of SST the weakest of the annual cycle. The weak zonal boreal spring gradient of SST reduces the intensity of the Walker circulation. Webster (1995) has hypothesized that this reduction in the intensity of the Walker circulation is an important factor that causes the predictability barrier of the coupled ocean–atmosphere system in the boreal spring. Cold SST is seen in the region

of Niño-1 and -2 during JJA and extends westward into the Niño-3 region during SON.

Accompanying the annual cycle in SST in the eastern tropical Pacific, the position of the ITCZ migrates meridionally about the equator. Coupled with such ITCZ shifts, the meridional wind over the region of Niño-3 undergoes significant change. During SON, the meridional wind contributes to divergence over the Niño-3 region where the SST has maximum interannual variability (Fig. 7, right). In contrast, during MAM, the surface meridional wind contributes to convergence over the Niño-3 region.

b. The interaction between the annual cycle and ENSO

Irrespective of the phase of ENSO, the annual cycle of the coupled ocean–atmospheric system predominates, driven by the annual migration of solar radiation. On the other hand, ENSO is basically driven by coupled ocean–atmosphere dynamic mechanisms in the tropical Pacific. Once an El Niño or La Niña anomaly starts to develop, it may be sustained for about a year. In this sense, the annual cycle and ENSO can be considered as two independent processes that take place simultaneously in the eastern tropical Pacific.¹ To first order, the magnitude of external atmospheric forcing is determined by the phase relationship between the annual cycle and the ENSO anomalies.

To see how the annual cycle interacts with ENSO, we examine the temporal variations in SST and atmospheric circulation over the eastern tropical Pacific Ocean (5°S–5°N, 160°–90°W). Figure 8 shows the time series of regional averages of the SST, precipitation and horizontal convergence in the surface meridional wind over this region. The convergence in the surface meridional wind is represented by the difference obtained by subtracting the spatial average of the wind over the southern part (0°–5°S) from the average over the northern part (0°–5°N) of the region. The time series covers the period from January 1979 to December 1992. Seasonal means were made for the seasons of DJF, MAM, JJA, and SON for each year. Using the seasonal means, we filtered out temporal variations of shorter time scales and focused on the annual cycle and interannual variation.

The annual cycle anomalies $\bar{X}'_s = \bar{X}_s - \bar{\bar{X}}$ of SST, precipitation, and meridional wind convergence are shown in panels at the right-hand side in Fig. 8. Driven by the annual cycle of solar radiation, the SST, precipitation, and meridional wind convergence have a consistent annual cycle. The annual cycle anomalies of all these components in the coupled system reach a maximum

positive value during MAM and a maximum negative value during SON. It is important to keep in mind that the annual cycle in the eastern tropical Pacific Ocean reaches opposite maxima during the two equinox seasons. This is a major factor that makes the seasonality of the SST-forced predictability during La Niña years differ from that during El Niño years.

The interannual variations in the SST, precipitation, and meridional wind convergence in the eastern tropical Pacific Ocean are further examined in Fig. 9, which shows the time series of the ENSO anomalies $X'_{s,y}$ [cf. Eq. (10)]. Based on the time series of the ENSO anomalies in the SST, the interannual variation in the eastern tropical Pacific Ocean during the period from 1979 to 1992 can be roughly divided into three warm events (DJF 1981/82 to SON 1983, DJF 1985/86 to SON 1987, and DJF 1990/91 to SON 1992) and three cold events (DJF 1979/80 to SON 1981, DJF 1983/84 to SON 1985, and DJF 1987/88 to SON 1989). Composite El Niño (La Niña) anomalies can be obtained by averaging the ENSO anomalies of the three warm (cold) events for each season:

$$[X'_s]_{\text{El Niño}} = \sum_{y=\text{El Niño}} X'_{s,y} \quad \text{and}$$

$$[X'_s]_{\text{La Niña}} = \sum_{y=\text{La Niña}} X'_{s,y}.$$

The composite ENSO anomalies of the three warm events and three cold events are also shown in Fig. 9 (right). The SST, precipitation, and meridional wind convergence have positive anomalies during El Niño years and negative anomalies during La Niña years. Notice that the largest ENSO precipitation anomaly occurs during MAM and the smallest ENSO precipitation anomaly occurs during SON. This feature is attributed to the phasing with annual cycle, which itself has a maximum precipitation during MAM and a minimum precipitation during SON over the eastern tropical Pacific Ocean.

The interaction between the annual cycle and ENSO is illustrated further in Figs. 10 and 11. Figure 10 compares the annual cycle anomalies (\bar{X}'_s) and the composite ENSO anomalies for El Niño years ($[X'_s]_{\text{El Niño}}$). Annual cycle anomalies are indicated by the left-side bars, and the composite ENSO anomalies are indicated by the right-side bars. During DJF and MAM, the annual cycle anomalies and the El Niño anomalies are of the same sign except for the SST during DJF. In contrast, during JJA and SON, the annual cycle anomalies are of opposite sign to the El Niño anomalies. Therefore, the annual cycle and the El Niño enhance each other during DJF and MAM but weaken each other during JJA and SON. Figure 11 compares the annual cycle anomalies (\bar{X}'_s) and the composite La Niña anomalies ($[X'_s]_{\text{La Niña}}$). Annual cycle and La Niña anomalies interfere with each other during DJF and MAM but enhance each other during JJA and SON. Figures 10 and 11 thus suggest one explanation for why El Niño increases atmospheric

¹ One explanation for the dynamic mechanism is the “delayed oscillator” (e.g., Battisti and Hirst 1989). It has also been suggested that ENSO is the exaggeration of the seasonal cycle (e.g., Philander 1990; Chang et al. 1995).

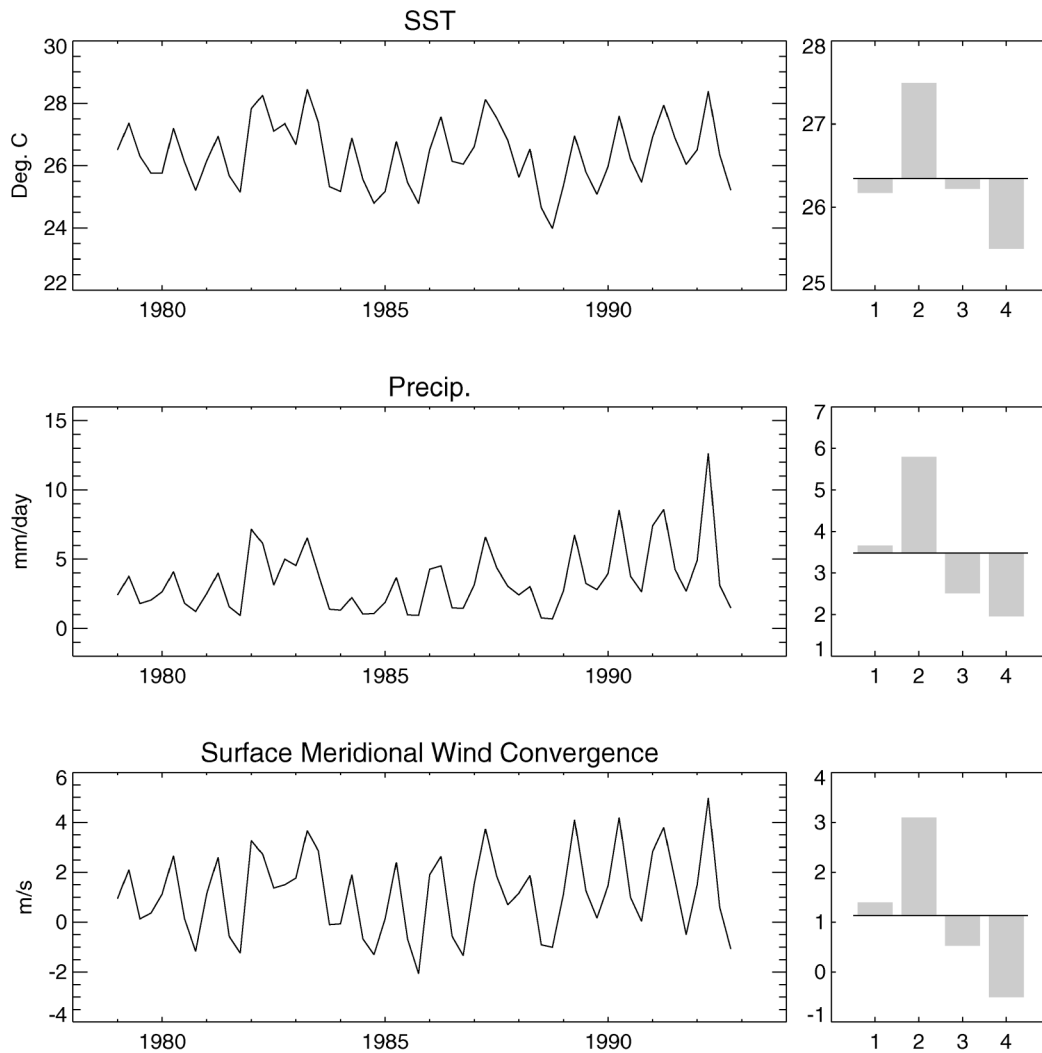


FIG. 8. Time series of the seasonal means (X_{s_j}) of the spatial average of the SST, precipitation, and the index of horizontal convergence of surface meridional wind over the eastern tropical Pacific (5°S – 5°N , 160° – 90°W). Climatological means for each variable are shown on the right. The numbers 1–4 under the right panels indicate the seasons of DJF, MAM, JJA, and SON, respectively.

predictability during the northern spring, while La Niña increases predictability during the northern autumn. For the same reason, one would expect to see the SST-forced atmospheric predictability to decrease during the autumn of El Niño years and the spring of La Niña years.

c. The concept of “ENSO-quark,” a useful paradigm for annual cycle–ENSO interaction

Interestingly, the interaction between the annual cycle and the interannual variability of ENSO can be represented by a schematic plot that mimics the concept of the “quark” model that is widely used in nuclear physics to explain the structure of nucleons and related phenomena. The schematic plot is shown in Fig. 12. The interaction between the annual cycle and El Niño is represented by the ovals and arrows in the left column.

The ovals are used to indicate anomalies of the SST with light shades for annual cycle and heavy shades for ENSO, and shaded ovals indicating warm SST anomalies, while hatched ovals indicate cold SST anomalies. The vertical arrows represent anomalies of precipitation with the dashed bar being used for the annual cycle and the solid bar being used for ENSO. An upward-pointing arrow represents an increase in precipitation, while a downward-pointing arrow represents a decrease in precipitation. The horizontal arrows represent anomalies in horizontal convergence in the surface meridional wind (a blank arrowhead for annual cycle and a filled arrowhead for ENSO), and the arrows pointing toward each other indicate anomalous convergence, while the arrows pointing away from each other indicate anomalous divergence. In brief, enhancement between the annual cycle and El Niño is indicated by arrows pointing in the

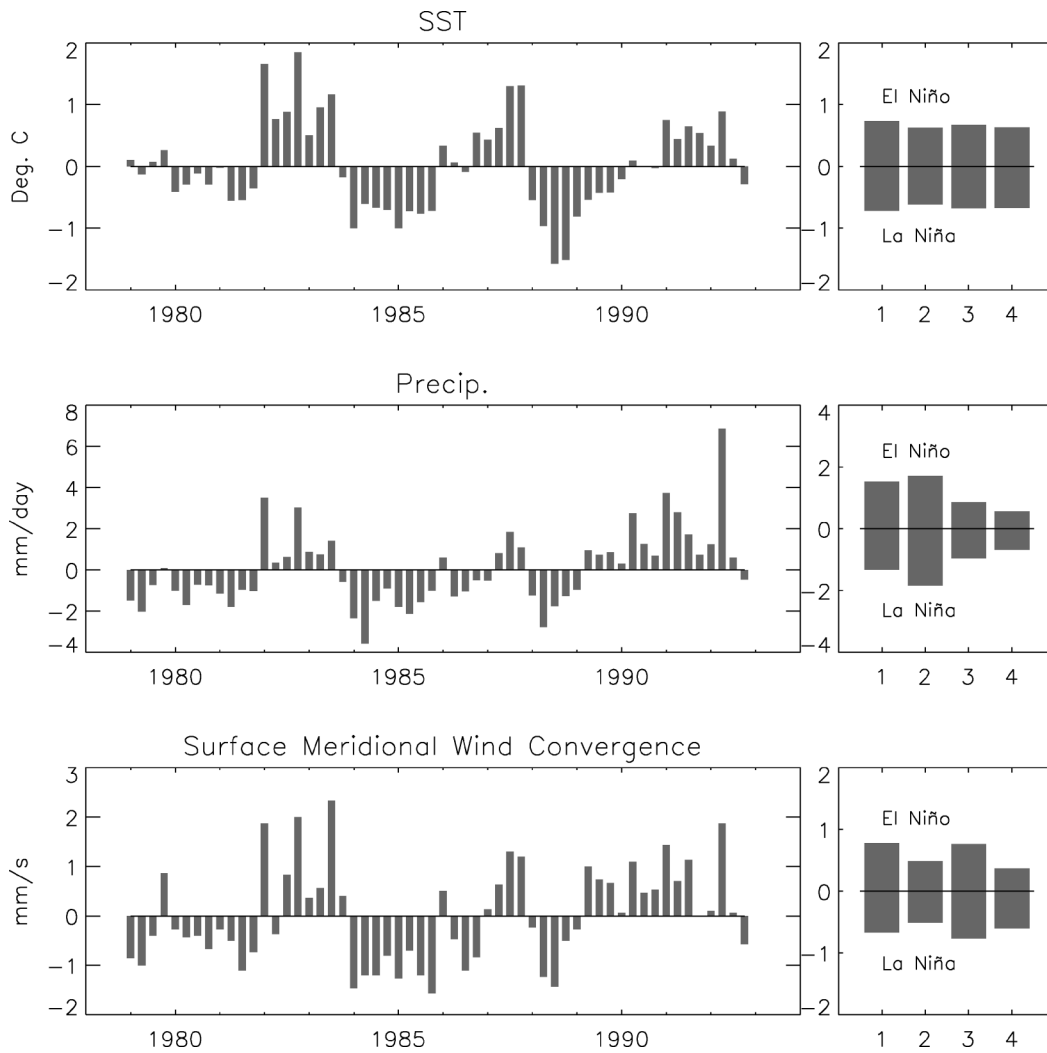


FIG. 9. Seasonal mean anomalies due to interannual variation X'_{xy} of (top) SST, (middle) precipitation, and (bottom) horizontal convergence of surface meridional wind. Composite anomalies for El Niño and La Niña events are shown on the right. The numbers 1–4 under the right panels indicate the seasons of DJF, MAM, JJA, and SON, respectively.

same direction and by ovals of the same type of shading. On the other hand, the weakening between the annual cycle and El Niño is indicated by the opposite directions of the arrows and different types of shading in the ovals. In the same manner, the interaction between the annual cycle and La Niña is represented by the ovals and arrows in the right column in Fig. 12.

Now, if one imagines each oval and its associated arrows to represent a quark (the oval representing its spin and the arrow representing its polarity) the annual cycle–ENSO interaction can be interpreted using the term “A-quark” to describe the state of annual cycle anomalies in the SST, precipitation, and meridional wind convergence, and “E-quark” to describe the state of the corresponding ENSO anomalies. Using the quark analogy, the statement, “The El Niño signal is enhanced when the annual cycle anomalies of SST, precipitation, and meridional wind convergence are of the same sign

as the ENSO anomalies,” can be restated as, “The signal of an El Niño or La Niña is enhanced when the polarities of the E-quark and A-quark are the same.”

d. Nonlinearity in the annual cycle–ENSO interaction

It is worth noting that the effect of the annual cycle–ENSO interaction is nonlinear. The nonlinearity is reflected in two phenomena: 1) the annual cycle–ENSO interaction has larger impact on the SST-forced atmospheric predictability during MAM than SON. For example, the predictability factor R for the MAM of 1983 is much larger than the R for MAM of 1989 in the tropical Pacific–American region (Fig. 4), and the difference between the R values for the two fall (SON) seasons of 1982 and 1988 is very small. 2) The SST-forced atmospheric predictability is generally weaker during the northern fall compared to other seasons (cf.

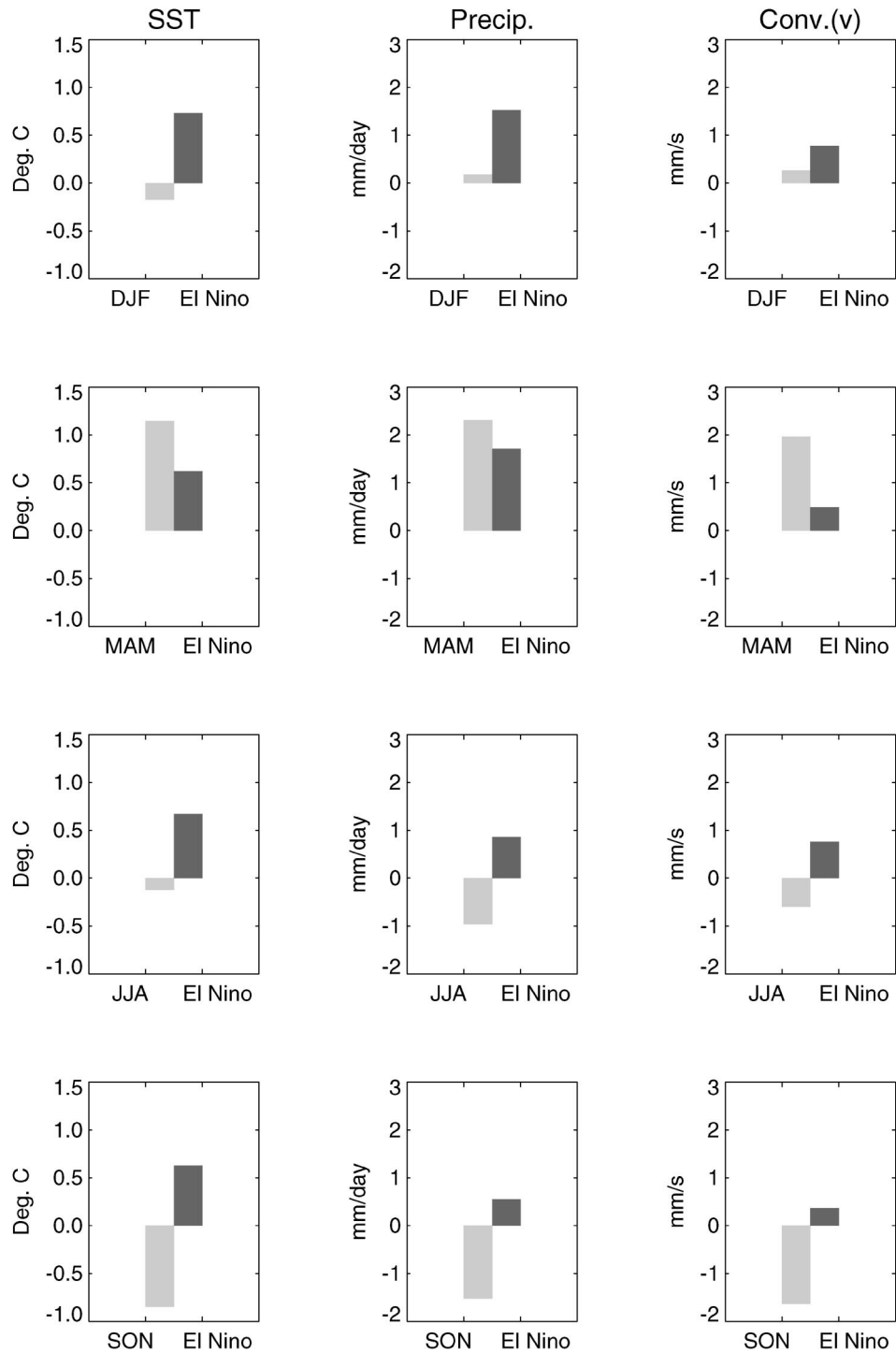


FIG. 10. Comparison of the seasonal mean anomalies due to annual cycle \bar{X}'_s and the seasonal mean anomalies due to interannual variability $[X'_s]$ El Niño averaged for the three La Niña events.

Table 3). In the above section, we have elucidated that the reduction of the SST-forced atmospheric predictability is mainly attributed to the weakening of the external variability. The fall weakening of the external variability can not be explained by the seasonality in

the SST variability itself because the weakest interannual variability in the tropical Pacific SST occurs in the northern spring (e.g., Rasmusson and Carpenter 1982; Chen and Van den Dool 1997; Fig. 1). An appropriate explanation for the two phenomena can be found in the

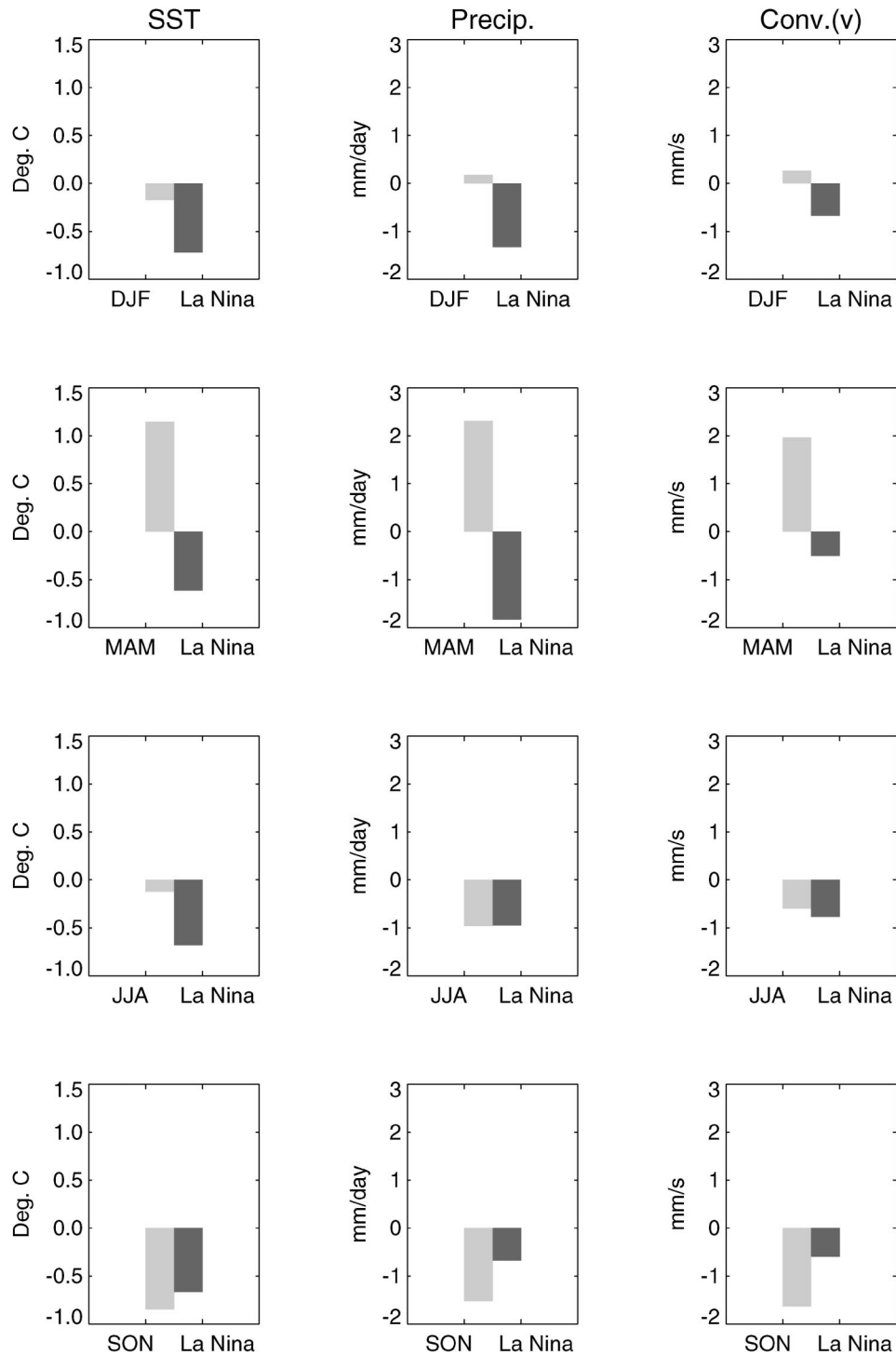


FIG. 11. Comparison of the seasonal mean anomalies due to annual cycle \bar{X}'_s and the seasonal mean anomalies due to interannual variability $[X'_s]$ La Niña averaged for the three La Niña events.

nonlinear regulation of water vapor condensation by the annual cycle in SST over the tropical Pacific Ocean. We have noticed that the SST is lowest in the eastern-central tropical Pacific during the northern fall due to annual cycle and is highest during the northern spring (Figs. 7 and

8). According to the Clausius–Clapeyron relation (e.g., Iribarne and Godson 1981), the same amount of change in temperature ΔT may cause much larger changes in evaporation or condensation in a warmer environment than it does in a colder environment, that is, $\Delta e/\Delta T|T_1$

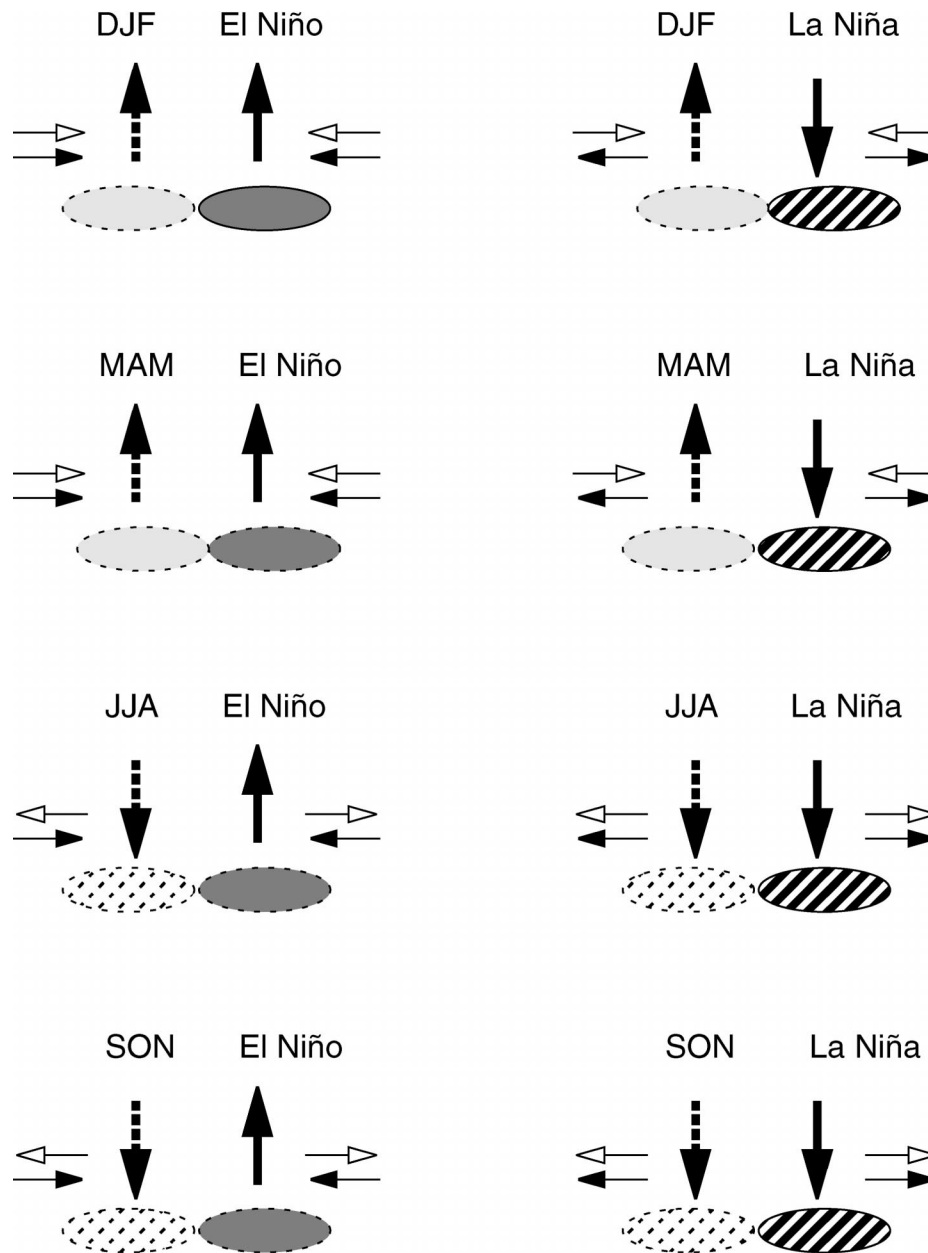


FIG. 12. Schematic chart illustrating modulation of annual cycle to interannual variation during (left) El Niño and (right) La Niña events over the tropical Pacific Ocean. Anomalies due to El Niño (La Niña) are indicated by the heavily shaded (hatched) ovals (SST) and solid arrows (vertical motions and horizontal convergence in the lower tropospheric meridional winds). Seasonal mean departures from the climatological annual mean are represented by the lightly shaded (hatched) ovals (SST) and the arrows with dashed bars (vertical motion) or empty heads (horizontal convergence in the meridional wind in the lower troposphere). The shading (hatching) is used to represent positive (negative) SST departures in the tropical Pacific Ocean (5°S – 5°N , 160° – 90°W).

$\ll \Delta e / \Delta T | T_2$, when $T_1 < T_2$. This nonlinearity can be seen in Fig. 9; the composite precipitation anomalies for the El Niño (La Niña) events is smallest (largest) during the northern fall (spring) when the SST annual cycle reaches its lowest (highest) point, although the corresponding composite anomalies of the SST and surface wind show much smaller differences. Since the

external forcing from SST is actually realized by the latent heat release during the process of water vapor condensation and by precipitation in the atmosphere, the magnitude of anomalous precipitation better represents the real external forcing by the atmospheric system. Therefore, one would expect to see that the warm El Niño SST anomalies induce larger external forcing

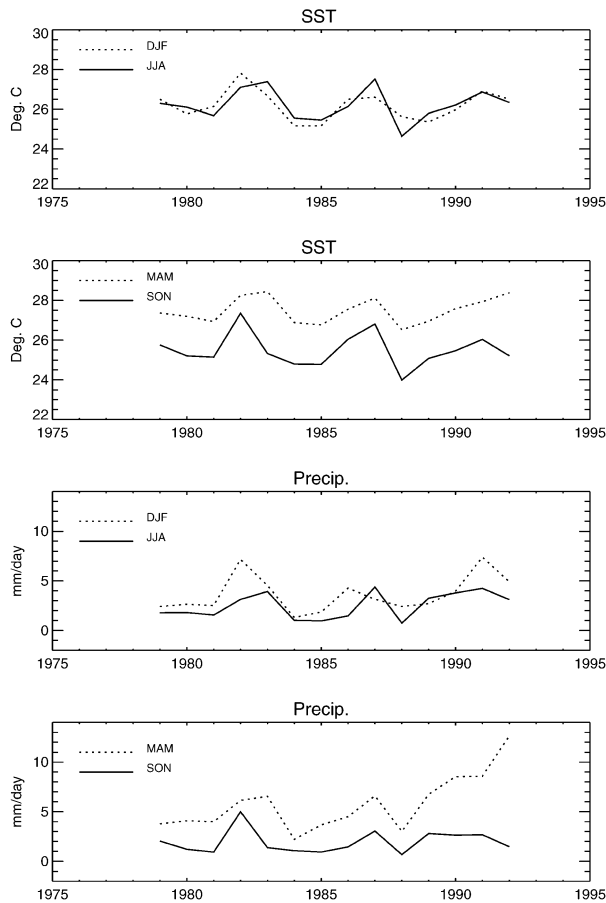


FIG. 13. Time series of seasonal means ($X_{s,t}$) of SST and precipitation. The interannual variations of the SST and precipitation are plotted for DJF and MAM by dotted lines and for JJA and SON by solid lines.

to the atmosphere during the northern spring than fall and that the interannual variation in SST has the weakest atmospheric response during the northern fall.

e. Seasonality in the effect of annual cycle–ENSO interaction

One may notice that the El Niño-forced and La Niña-forced atmospheric predictabilities have the largest difference over the tropical Pacific during MAM (Fig. 4). On the other hand, the SST-forced atmospheric predictability is weakest over the tropical Pacific during SON (Table 3). The two phenomena reflect seasonality in the interaction between the annual cycle and ENSO. Figure 13 compares the interannual variation of SST and precipitation for MAM and SON, and JJA and DJF, respectively. One can see that the curves of interannual variation of SST and precipitation in MAM are clearly separated from those of SON. The MAM–SON separation indicates that the physical environment for an ENSO during MAM is quite different from that during SON. During MAM (SON) the SST becomes warmest

(coldest) in a year and the meridional wind convergence and precipitation reach an annual maximum (minimum) over the tropical eastern Pacific (Fig. 8). The physical environment during MAM (SON) provides a favorable background condition for an El Niño to produce stronger (weaker) anomalies in the atmosphere and thus higher (lower) predictability. Hence, the effect of the annual cycle–ENSO interaction becomes more apparent when the two equinoctial seasons are compared. In contrast, the annual cycle–induced DJF – JJA differences in the SST, meridional wind convergence, and precipitation are much smaller. That is, the differences in background conditions for an El Niño anomalous event are smaller when the DJF and JJA seasons are compared. Thus, the effect of the annual cycle–ENSO interaction is less significant when the two solstice seasons are compared.

f. The El Niño/La Niña difference in the extratropical predictabilities

As we have discussed in section 3, the SST-forced atmospheric predictability has a similar seasonality in the extratropics as that in the Tropics (Fig. 4) because the predictability in the extratropics mainly comes from the response to the interannual variation in tropical Pacific SST. However, in addition to the annual cycle–ENSO interaction discussed above, the seasonality in atmospheric planetary waves is another important factor that determines the atmospheric seasonal predictability in the extratropics. It is the seasonality in planetary waves that makes the annual variation of the predictability in the northern extratropics very different from the Tropics and southern extratropics during the 1988/89 La Niña year (see also section 3b). In addition, it is also worth noting that the nonlinear asymmetry between El Niño and La Niña also exists in the teleconnections associated with them (e.g., Hoerling et al. 1997).

5. Conclusions

In this paper, an effort has been made to obtain a better understanding of the SST-forced atmospheric “short-term climate” predictability. The term short-term climate is used here to represent climate variation on seasonal-to-interannual time scales.

Output from the ensemble seasonal forecasts of an ECMWF AGCM has been analyzed. By introducing a normalized signal-to-noise ratio (R) to measure the predictability, we found the following features in the spatial structure and temporal evolution of the SST-forced atmospheric short-term climate predictability: the predictability is (i) greater in the Tropics than in the extratropics, (ii) greater over the Pacific and Atlantic than over the Indian Ocean and the Asian monsoon region, and (iii) greater in the winter hemisphere than in the summer hemisphere. (iv) The predictability is weakest during northern fall, and (v) the 1982/83 strong El Niño event forced larger atmospheric predictability during the

northern spring than fall, while the opposite occurred during the 1988/89 strong La Niña event—the same results as found, for example, by Chen and Van den Dool (1997).

The nature of the temporal and spatial structure in the SST-forced atmospheric short-term climate variability is explored further by partitioning the predictability into its internal and external components. The basic assumption is that external variability is determined by the prescribed forcing given by the evolving SST, and the internal variability represents the sensitivity to initial conditions. It is found that the temporal and spatial variation in the predictability is mainly determined in the Tropics by the external variability, that is, by SST forcing. In the extratropics, the variations in the predictability are determined by the variations of both the internal and external variabilities. It is also found that the seasonality of the internal variability differs from that of the external variability in the extratropics. The internal variability is larger in the northern extratropics during the northern fall and larger in the southern extratropics during the boreal spring. An opposite asymmetry between the two equinox seasons is seen in the external variability. It is the conjunction of the increase in the internal variability and the decrease in the external variability that make the predictability particularly weak in the northern extratropics during the boreal fall. Yet, why the seasonal variation in the internal variability differs from that in the external variability in the extratropics is a new question remaining to be solved.

An attempt is made to find mechanisms that determine the seasonality of the SST-forced atmospheric predictability. In this paper, we focus on the SST forcing and the atmospheric external variability over the tropical Pacific Ocean. We find it appropriate to use the annual cycle–ENSO interaction over the tropical Pacific Ocean to explain why stronger SST-forced atmospheric predictability is observed in the spring during El Niño years while stronger predictability occurs in the fall during La Niña years. In the eastern tropical Pacific Ocean, the SST tends to be higher during the spring but lower during the fall. Therefore, the forcing of warm SST during an El Niño year is further enhanced by the annual cycle during the spring but weakened during the autumn. In contrast, the forcing of cold SST during a La Niña year is weakened during the spring but enhanced during autumn. A conceptual model is introduced to help explain the annual cycle–ENSO interaction. Also, the model shows some interesting analogies to the quark model in nuclear physics.

The weakest atmospheric predictability in the northern fall can be explained by the nonlinearity of the hydrological processes associated with the annual cycle–ENSO interaction. Interannual variability of the precipitation (representing thermal forcing in the atmosphere) over the tropical Pacific Ocean is weakest during the fall because the SST is coldest compared to other sea-

sons. Therefore, the signal of the external forcing (atmospheric response to SST variation), and hence the SST-forced atmospheric predictability, is the weakest during the northern fall. The seasonality in atmospheric planetary waves is another factor that makes the SST-forced atmospheric predictability particularly weak in the northern extratropics during the northern fall.

The above conclusions are drawn from the analysis based on ensemble simulations of one atmospheric model. In this paper, we do not attempt to answer questions such as whether the model's internal variability is comparable to natural variability or whether the model's sensitivity to external forcing fully represents the sensitivity of the atmospheric circulation in the real world. However, consistency among the results from this model (this paper) and other models (e.g., Chen and Van den Dool 1997; Kumar and Hoerling 1998) suggests some generality of the conclusions presented here.

Acknowledgments. Funding for this research was obtained through a grant from the Climate Dynamics Division of the National Science Foundation (ATM-0120956). The authors would like to thank Martin Hoerling for reading through the manuscript and Grant Branstator, Prashant Sardeshmukh, and two anonymous reviewers for helpful comments and suggestions concerning this work. Support to the first author by Maurice Blackmon and Clara Deser is gratefully acknowledged.

REFERENCES

- Anderson, J., H. Van den Dool, A. Barnston, W. Chen, W. Stern, and J. Plushay, 1999: Present-day capabilities of numerical and statistical models for atmospheric extratropical seasonal simulation and prediction. *Bull. Amer. Meteor. Soc.*, **80**, 1349–1361.
- Arakawa, A., 1972: Design of the UCLA general circulation model. Numerical Simulation of Weather and Climate, Tech. Rep. 7, Dept. of Meteorology, University of California, Los Angeles, 116 pp.
- Battisti, D. S., and A. C. Hirst, 1989: Interannual variability in the tropical atmosphere–ocean model: Influence of the basic state, ocean geometry and nonlinearity. *J. Atmos. Sci.*, **46**, 1678–1712.
- Becker, B. D., 1997: The ECMWF Ensemble Simulation CD-ROMs. European Centre for Medium-Range Weather Forecasts, Shinfield Park, Reading, Berkshire, United Kingdom. [Available online at <http://www.ecmwf.int>.]
- Blackmon, M. L., J. E. Geisler, and E. J. Pitcher, 1983: A general circulation model study of January climate anomaly patterns associated with interannual variation of equatorial Pacific sea surface temperatures. *J. Atmos. Sci.*, **40**, 1410–1425.
- Borges, M. D., and P. D. Sardeshmukh, 1995: Barotropic Rossby wave dynamics of zonally varying upper-level flows during northern winter. *J. Atmos. Sci.*, **52**, 335–354.
- Brankovic, C., and T. N. Palmer, 1997: Atmospheric seasonal predictability and estimates of ensemble size. *Mon. Wea. Rev.*, **125**, 859–874.
- , —, and L. Ferranti, 1994: Predictability of seasonal atmospheric variations. *J. Climate*, **7**, 217–237.
- Chang, P., L. Ji, B. Wang, and T. Li, 1995: Interaction between the seasonal cycle and El Niño–Southern Oscillation in an intermediate coupled ocean–atmosphere model. *J. Atmos. Sci.*, **52**, 2353–2372.
- Charney, J. G., 1949: On a physical basis of numerical prediction of large-scale motions in the atmosphere. *J. Meteor.*, **6**, 371–385.

- , and N. A. Phillips, 1953: Numerical integration of the quasi-geostrophic equations for barotropic and simple baroclinic flows. *J. Meteor.*, **10**, 71–99.
- , and J. Shukla, 1981: Predictability of monsoons. *Monsoon Dynamics*, J. Lighthill and R. F. Pearce, Eds., Cambridge University Press, 99–110.
- , R. Fjørtoft, and J. von Neumann, 1950: Numerical integration of the barotropic vorticity equation. *Tellus*, **2**, 237–254.
- Chen, W. Y., 1989: Estimate of dynamical predictability from NMC DERF experiments. *Mon. Wea. Rev.*, **117**, 1227–1236.
- , and H. M. Van den Dool, 1997: Atmospheric predictability of seasonal, annual, and decadal climate means and the role of the ENSO cycle: A model study. *J. Climate*, **10**, 1236–1254.
- Dalcher, A., and E. Kalnay, 1987: Error growth and predictability in operational ECMWF forecasts. *Tellus*, **39A**, 474–491.
- Diaz, H. F., and V. Markgraf, 2000: *El Niño and the Southern Oscillation: Multiscale Variability and Global and Regional Impacts*. Cambridge University Press, 496 pp.
- Hoerling, H. P., A. Kumar, and M. Zhong, 1997: El Niño, La Niña, and the nonlinearity of their teleconnections. *J. Climate*, **10**, 1769–1786.
- Horel, J. D., and J. M. Wallace, 1981: Planetary-scale atmospheric phenomena associated with the Southern Oscillation. *Mon. Wea. Rev.*, **109**, 813–829.
- Hoskins, B. J., and D. J. Karoly, 1981: The steady linear response of a spherical atmosphere to thermal and orographic forcing. *J. Atmos. Sci.*, **38**, 1179–1196.
- Iribarne, J. V., and W. L. Godson, 1981: *Atmospheric Thermodynamics*. D. Reidel, 259 pp.
- Kasahara, A., and W. M. Washington, 1967: NCAR global general circulation model of the atmosphere. *Mon. Wea. Rev.*, **95**, 389–402.
- Kumar, A., and M. P. Hoerling, 1998: Annual cycle of Pacific–North American seasonal predictability associated with different phases of ENSO. *J. Climate*, **11**, 3295–3308.
- Kurihara, Y., 1965: Numerical integration of the primitive equations on a spherical grid. *Mon. Wea. Rev.*, **93**, 399–415.
- Lau, N.-C., 1985: Modeling the seasonal dependence of the atmospheric responses to observed El Niño 1962–1976. *Mon. Wea. Rev.*, **113**, 1970–1996.
- Livezey, R. E., M. Masutani, A. Leetmaa, H. Rui, M. Ji, and A. Kumar, 1997: Teleconnective response of the Pacific–American region atmosphere to large central equatorial Pacific SST anomalies. *J. Climate*, **10**, 1787–1820.
- Lorenz, E. N., 1960: Energy and numerical weather prediction. *Tellus*, **12**, 364–411.
- , 1963: Deterministic nonperiodic flow. *J. Atmos. Sci.*, **20**, 130–141.
- , 1982: Atmospheric predictability experiments with a large numerical model. *Tellus*, **34**, 505–513.
- Miyakoda, K., G. D. Hembere, R. F. Striker, and I. Shulman, 1972: Cumulative results of extended forecast experiments. Part I: Model performance for winter cases. *Mon. Wea. Rev.*, **100**, 836–855.
- Palmer, T. N., 1994: Chaos and predictability in forecasting the monsoons. *Proc. Indian Natl. Sci. Acad.*, **60A**, 57–66.
- , and S. Tibaldi, 1988: On the prediction of forecast skill. *Mon. Wea. Rev.*, **116**, 2453–2480.
- , and D. L. T. Anderson, 1994: The prospects for seasonal forecasting—A review paper. *Quart. J. Roy. Meteor. Soc.*, **120**, 755–793.
- Philander, S. G., 1990: *El Niño, La Niña, and the Southern Oscillation*. Academic Press, 293 pp.
- Phillips, N. A., 1959: Numerical integration of the primitive equations on the hemisphere. *Mon. Wea. Rev.*, **87**, 109–120.
- Rasmusson, E. M., and T. H. Carpenter, 1982: Variations in tropical sea surface temperature and surface wind fields associated with the Southern Oscillation/El Niño. *Mon. Wea. Rev.*, **110**, 354–384.
- Reynolds, C. A., P. J. Webster, and E. Kalnay, 1994: Random error growth in NMC's global forecasts. *Mon. Wea. Rev.*, **122**, 1281–1305.
- Richardson, L. F., 1922: *Weather Prediction by Numerical Process*. Cambridge University Press, 236 pp.
- Rowell, D. P., 1998: Assessing potential seasonal predictability with an ensemble of multidecadal GCM simulations. *J. Climate*, **11**, 109–120.
- Schubert, S. D., and M. Suarez, 1989: Dynamical predictability in a simple general circulation model: Average error growth. *J. Atmos. Sci.*, **46**, 353–370.
- Shukla, J., 1981: Dynamic predictability of monthly means. *J. Atmos. Sci.*, **38**, 2547–2572.
- , and J. M. Wallace, 1983: Numerical simulation of the atmospheric response to equatorial Pacific sea surface temperature anomalies. *J. Atmos. Sci.*, **40**, 1613–1630.
- Shuman, F. G., and J. B. Hovermale, 1968: An operational six-layer primitive equation. *J. Appl. Meteor.*, **7**, 525–547.
- Smagorinsky, J. S., S. Manabe, and J. L. Holloway, 1965: Numerical results from a ninelevel general circulation model of the atmosphere. *Mon. Wea. Rev.*, **93**, 727–768.
- Tracton, M. S., K. Mo, W. Chen, E. Kalnay, R. Kistler, and G. White, 1989: Dynamical extended range forecasting (DERF) at the National Meteorological Center. *Mon. Wea. Rev.*, **117**, 1604–1635.
- Trenberth, K. E., 1984: Signal versus noise in the Southern Oscillation. *Mon. Wea. Rev.*, **112**, 326–332.
- Van den Dool, H. M., 1994: Long range weather forecasts through numerical and empirical methods. *Dyn. Atmos. Oceans*, **20**, 247–270.
- von Neumann, J., and R. D. Ritchmyer, 1950: A method for the numerical calculation of hydrodynamical shocks. *J. Appl. Phys.*, **21**, 232–237.
- Wallace, J. M., E. M. Rasmusson, T. P. Mitchell, V. E. Kousky, E. S. Sarachik, and H. von Storch, 1998: On the structure and evolution of ENSO-related climate variability in the tropical Pacific: Lessons from TOGA. *J. Geophys. Res.*, **103C**, 14 241–14 260.
- Webster, P. J., 1982: Seasonality in the local and remote atmospheric response to sea surface temperature anomalies. *J. Atmos. Sci.*, **39**, 41–52.
- , 1995: The annual cycle and the predictability of the tropical coupled ocean-atmosphere system. *Meteor. Atmos. Phys.*, **56**, 33–55.
- , and T. P. Palmer, 1997: The past and future of El Niño. *Nature*, **390**, 562–564.
- , V. O. Magaña, T. N. Palmer, R. A. Thomas, M. Yanai, and T. Yasunari, 1998: Monsoons: Process, predictability, and prospects for prediction. *J. Geophys. Res.*, **103D**, 14 451–14 510.